J. Fluid Mech. (2015), *vol.* 771, *pp.* 407–423.
doi:10.1017/jfm.2015.182

Sources and fluxes of scale energy in the overlap layer of wall turbulence

A. Cimarelli[1], E. De Angelis[2,†], P. Schlatter[3], G. Brethouwer[3], A. Talamelli[2] and C. M. Casciola[4]

[1]CIRI – Aeronautica, Università di Bologna, Via Fontanelle 40, 47121 Forlì FC, Italy

[2]Dipartimento di Ingegneria Industriale, Università di Bologna, Via Fontanelle 40, 47121 Forlì FC, Italy

[3]Linné FLOW Centre, KTH Mechanics, SE-100 44 Stockholm, Sweden

[4]Dipartimento di Ingegneria Meccanica e Aerospaziale, Università di Roma 'La Sapienza', Piazzale Aldo Moro 5, 00185 Rome, Italy

(Received 3 July 2014; revised 15 January 2015; accepted 18 March 2015; first published online 20 April 2015)

Direct numerical simulations of turbulent channel flows at friction Reynolds numbers (*Re*) of 550, 1000 and 1500 are used to analyse the turbulent production, transfer and dissipation mechanisms in the compound space of scales and wall distances by means of the Kolmogorov equation generalized to inhomogeneous anisotropic flows. Two distinct peaks of scale-energy source are identified. The first, stronger one, belongs to the near-wall cycle. Its location in the space of scales and physical space is found to scale in viscous units, while its intensity grows slowly with *Re*, indicating a near-wall modulation. The second source peak is found further away from the wall in the putative overlap layer, and it is separated from the near-wall source by a layer of significant scale-energy sink. The dynamics of the second outer source appears to be strongly dependent on the Reynolds number. The detailed scale-by-scale analysis of this source highlights well-defined features that are used to make the properties of the outer turbulent source independent of Reynolds number and wall distance by rescaling the problem. Overall, the present results suggest a strong connection of the observed outer scale-energy source with the presence of an outer region of turbulence production whose mechanisms are well separated from the near-wall region and whose statistical features agree with the hypothesis of an overlap layer dominated by attached eddies. Inner–outer interactions between the near-wall and outer source region in terms of scale-energy fluxes are also analysed. It is conjectured that the near-wall modulation of the statistics at increasing Reynolds number can be related to a confinement of the near-wall turbulence production due to the presence of increasingly large production scales in the outer scale-energy source region.

Key words: turbulent boundary layers, turbulent flows

1. Introduction

One of the most peculiar aspects of turbulence in wall-bounded flows is the ability of the turbulent fluctuations to regenerate themselves through self-sustained processes.

† Email address for correspondence: e.deangelis@unibo.it

In wall flows, the production of turbulent fluctuations is embedded in the system instead of being provided by an external agent. The dynamics of these self-sustaining mechanisms has been extensively investigated over the past 30 years, since these processes are responsible for the energy drain from the mean flow to the fluctuating field and for the turbulent drag.

It has long been understood that the near-wall layer, being the site of the highest rate of turbulent energy production and of the maximum turbulent intensities, is crucial to the dynamics of attached shear flows. The possibility to identify robust kinematic features in the proximity of a wall fed the hope of the scientific community to obtain a complete and consistent dynamical description of the underlying physics of these processes. The turbulent fluctuations near a wall have been found to organize in well-defined coherent motions consisting of quasi-streamwise vortices and high/low-velocity regions alternating in the spanwise direction. The former are longitudinal vortices with typical streamwise and spanwise length scales $\lambda_x^+ \approx 200$ and $\lambda_z^+ \approx 50$, respectively (hereafter a superscript $+$ will denote the so-called inner units; see e.g. Townsend 1976), slightly tilted away from the wall. The latter are long and wide alternating arrays of streamwise streaks of local velocity excess/defect, with length scales $\lambda_x^+ \approx 1000$ and $\lambda_z^+ \approx 100$, superimposed on the mean flow. These features have been recognized in several numerical and experimental works (see e.g. Kim, Kline & Reynolds 1971; Smith & Metzler 1983; Robinson 1991). From these observations, several scientists tried to derive a conceptual model of these processes. Following the work of Jiménez & Pinelli (1999), the continuous creation and destruction of these turbulent structures form a self-sustaining cycle maintaining near-wall turbulence without the need of any input from the core flow, i.e. it is an autonomous cycle. The streamwise vortices extract energy from the mean flow to create alternating streaks of longitudinal velocity. Presumably by inflectional instabilities, these streaks in turn give rise to the vortices closing the cycle (see also Hamilton, Kim & Waleffe 1995; Jeong *et al.* 1997; Schoppa & Hussain 2002).

From a more applied point of view, the near-wall cycle is crucial, since it controls the magnitude of the wall stress. But coherent structures exist also at larger scales in the so-called overlap layer (Hutchins & Marusic 2007*a*,*b*; Jiménez & Hoyas 2008), and have recently been suggested to form an outer self-sustaining mechanism of regeneration of very large turbulent fluctuations (see e.g. Flores & Jiménez 2006; Hwang & Cossu 2010; Mizuno & Jiménez 2013). The phenomenology resembles the self-regenerating cycle near the wall though its characteristic dimensions are larger (see e.g. del Alamo *et al.* 2006; Monty *et al.* 2007). The coherent motions involved in this outer cycle should scale with external variables, meaning that their dimensions and action should increase as the extent of the log layer widens with Reynolds number. Hence, the understanding of these outer dynamics is crucial for the modelling of wall turbulence in the asymptotic regime of very large Reynolds number. Furthermore, its analysis could help to clarify the interactions between the outer and inner regions of wall flows needed in the formulation of near-wall models for large-eddy simulations (see e.g. Piomelli & Balaras 2002), and to explain the controversial mixed inner/outer scaling of the near-wall quantities such as spectra and turbulent intensities (see e.g. Hutchins & Marusic 2007*b*; DeGraaff & Eaton 2000).

Generally speaking, the problem of wall turbulent flows has been classically studied by dividing the flow domain into well-characterized regions depending on wall distance. In particular, wall-bounded flows are divided into a near-wall inner region and an outer region populated by large structures. These two distinct regions are present in all wall-bounded flows and interact in the overlap region. While in the

outer flow the velocity profile depends on the particular flow configuration, in the inner and overlap regions it exhibits a high degree of universality starting linearly from the wall and then approaching a logarithmic behaviour. These behaviours opportunely scaled with viscous units should collapse for different flows and different Reynolds numbers; see Nagib & Chauhan (2008) for a detailed description of the controversies on this topic. The same scaling should apply to the turbulent intensity profiles and to all the statistical observables of the inner region.

However, the near-wall quantities exhibit a Reynolds-number dependence as shown by the fact that the energy of the long turbulent fluctuations of the overlap layer grows when the Reynolds number increases. This large-scale motion is found to actively modulate the near-wall turbulence by production of near-wall scales at increasing Reynolds number (Hutchins & Marusic 2007*b*). The observed increase of the streamwise turbulent fluctuation peak, the possible appearance of a second peak in the overlap flow and the presence of a marked outer-scale peak in the energy spectrum are thought to be a signature of these effects. An important consequence of the Reynolds-number dependence of the large turbulent motion in the overlap layer is that most of the turbulence production should asymptotically come from this region owing to the widening of the overlap layer with Re (Smits, McKeon & Marusic 2011). Even if no Reynolds-number dependence for the outer turbulent production intensity is expected, the outer turbulent self-sustained mechanisms are thought to dominate the high-Reynolds-number asymptotic state of wall turbulence.

Given the Reynolds-number dependence of these processes in the compound scale/physical space, an interesting approach to study the basic mechanisms of the outer cycle has recently been proposed in Cimarelli, De Angelis & Casciola (2013) by extending the statistical approach used in Marati, Casciola & Piva (2004) and applied by Saikrishnan *et al.* (2012) to moderately high-Reynolds-number data. The classical approach for addressing these issues in channel flow is based on a Fourier decomposition along the homogeneous directions while keeping a description in terms of the physical distance in the wall-normal direction (see e.g. del Alamo *et al.* 2004). However, this more traditional approach does not allow for a net distinction between position in the wall-normal direction and wall-normal scale at which energy generation and energy flux take place. The tool used here to describe the energy content associated with a given scale of motion in a given position in space is based, instead, on the generalization of the Kolmogorov equation for the second-order structure function, originally introduced for homogeneous and isotropic turbulence, and successively extended to inhomogeneous anisotropic flows by Hill (2002). The generalized Kolmogorov equation keeps the two concepts of wall-normal position and wall-normal scale clearly distinct, thereby allowing one to distinguish between the two associated components of the energy flux. In Cimarelli *et al.* (2013), this multidimensional description of turbulence has been used and proven fundamental for the understanding of the wall turbulent physics and for its modelling as shown in Cimarelli & De Angelis (2011). In the present paper, we extend this work by analysing how the turbulent energy associated with a certain scale (scale energy) is generated, transferred and dissipated among different scales and wall distances on varying the Reynolds number, with particular attention being paid to the outer self-regeneration mechanisms.

2. Direct numerical simulation database and single-point statistics

In the present study, we analyse data of three direct numerical simulations (DNS) of fully developed turbulent channel flow at $Re_\tau = u_\tau h/\nu = 550$, 1000 and 1500,

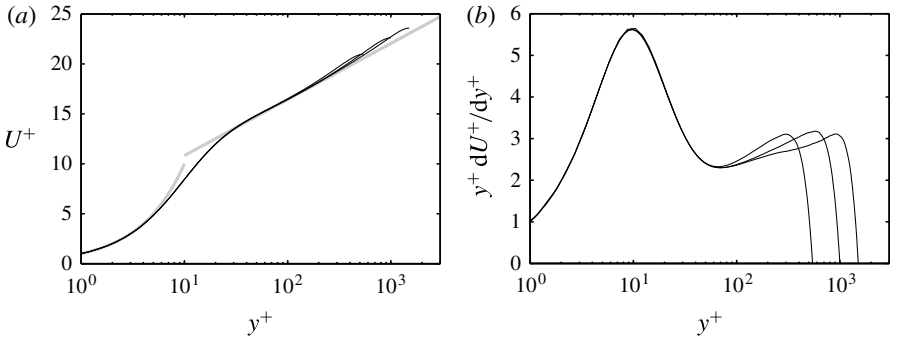

FIGURE 1. Mean velocity profiles $U^+(y^+)$ and (premultiplied) mean velocity gradient $y^+\mathrm{d}U^+/\mathrm{d}y^+$ for the three channel DNS considered in this study, with $Re_\tau = 550$, 1000 and 1500. Here $U^+(y^+) = y^+$ and $U^+(y^+) = 1/\kappa \log(y^+) + B$ with $\kappa = 0.41$ and $B = 5.2$ are indicated by thick grey lines.

Case	Re_τ	L_x	L_y	L_z	$N_x \times N_y \times N_z$	Δx^+	Δz^+
DNS550	550	$8\pi h$	$2h$	$4\pi h$	$1024 \times 257 \times 1024$	13.5	6.7
DNS1000	1000	$8\pi h$	$2h$	$3\pi h$	$2560 \times 385 \times 1920$	9.8	4.9
DNS1500	1500	$12\pi h$	$2h$	$10.5h$	$6144 \times 577 \times 3456$	9.2	4.5

TABLE 1. Parameters of the simulations: Re_τ is the friction Reynolds number; L_x, L_y and L_z are the lengths of the computational domain in the streamwise (x), wall-normal (y) and spanwise (z) directions; N_x, N_y and N_z are the number of points in physical space; and Δ_x^+, Δ_y^+ and Δ_z^+ are the corresponding grid spacings in viscous units.

respectively. Here, u_τ is the friction velocity, h the channel half gap width and ν the viscosity. The simulations were carried out with a pseudo-spectral code using Fourier expansions and dealiasing in the homogeneous directions, and Chebyshev polynomials in the wall-normal direction. Full details of the algorithm can be found in Chevalier *et al.* (2007). The domain size and resolution of the three DNS are given in table 1. Data of the DNS at $Re_\tau = 550$ and 1000 have already been used for studies of wall turbulence in Cimarelli *et al.* (2013) and Lenaers *et al.* (2012), respectively. Let us mention that the lower resolution adopted for the simulation of the lower-Reynolds-number case at $Re_\tau = 550$ has been tested and found not to affect the statistical quantities we are analysing in the present work.

Profiles of the streamwise mean velocity and the log-law indicator function of the three DNS are shown in figure 1. The near-wall region has obviously a very high degree of similarity for the three Reynolds numbers, while outside the buffer layer, in the overlap layer, differences due to Reynolds number effects become visible. A tentative plateau in the indicator function profile starts to appear with increasing Re_τ but is not yet clearly present, meaning that a true logarithmic layer is absent even at the highest Re_τ.

The single-point turbulent kinetic energy balance compacts in a simple way the overall multidimensional behaviour of turbulence describing the energetics only in physical space. For the symmetries of the channel, this equation reads

$$\frac{\mathrm{d}\psi}{\mathrm{d}y} = s(y), \tag{2.1}$$

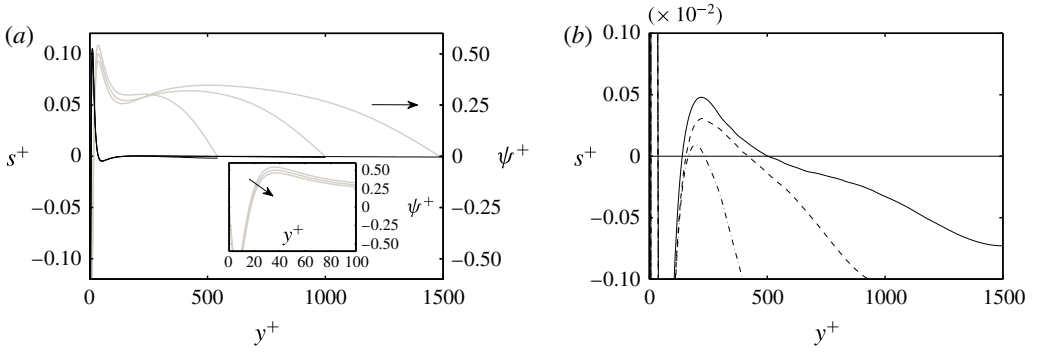

FIGURE 2. (*a*) Source term of the kinetic energy budget s^+ (black lines) and corresponding spatial flux ψ^+ (grey lines) for the three Reynolds numbers $Re_\tau = 550$, 1000 and 1500. The inset shows a zoom of the near-wall peak of the spatial flux ψ^+. The two arrows indicate increasing Reynolds numbers. (*b*) Magnification of the region around the second positive peak of s. Increasing Re_τ from dash-dotted to dashed and solid lines.

and describes how turbulent energy is redistributed among different wall distances y through the spatial flux $\psi = (\langle u_i^2 v\rangle + \langle pv\rangle/\rho - \nu \mathrm{d}\langle u_i^2\rangle/\mathrm{d}y)$ from the production to the dissipation regions of the flow defined by positive and negative values of the source term $s(y) = -\langle uv\rangle(\mathrm{d}U/\mathrm{d}y) - \langle\epsilon\rangle$. Hereafter, $\langle\cdot\rangle$ will be used to denote ensemble average. As shown by the black lines in figure 2(*a*), in wall turbulence the energy source is near the wall in the so-called buffer layer. In this layer, turbulence production exceeds the local dissipation. Conversely, the wall and bulk flow behave as sink regions dissipating turbulent energy emerging from the buffer layer through the spatial energy flux; see grey lines in figure 2(*a*). Indeed, the spatial flux is zero at the peak of the energy source and becomes positive (towards the core flow) further away from the wall and negative (towards the wall) closest to the wall. Actually, in between the buffer layer and the core of the flow, a third region can be defined, the so-called overlap layer, which is the main subject of the present work. Although this region is expected to be an equilibrium layer where production and dissipation locally balance, production is actually larger than dissipation, leading to an outer energy source; see figure 2(*b*). The understanding of this region of the flow is very important especially when dealing with the high-Reynolds-number state of wall turbulence. Even if its intensity is very small compared to the one near the wall, this outer energy source shows an apparent Re dependence; see again figure 2(*b*). In particular, it appears that, by increasing the Reynolds number, the role of the outer energy source becomes more important. By defining the overall inner and outer energy source as the integral of the source $s(y)$ restricted to the two (inner and outer) regions where $s(y) > 0$, respectively,

$$\Xi_{inn} = \int_y s(y)\mathrm{d}y \quad y \in \{\text{inner region of energy source } s(y) > 0\},$$
$$\Xi_{out} = \int_y s(y)\mathrm{d}y \quad y \in \{\text{outer region of energy source } s(y) > 0\},$$

we can roughly estimate the relative importance of the two regions as a function of Reynolds number by means of the ratio Ξ_{out}/Ξ_{inn}. The present data show a significant increase of this ratio from 0.0031 at $Re_\tau = 550$ to 0.0347 and 0.0617 at $Re_\tau = 1000$ and 1500, respectively. Extrapolating this trend, one can expect the outer

source to become dominant above $Re_\tau = 15\,000$–$20\,000$. The increased intensity of the outer source also has consequences for the topology of the energy transfer. Indeed, as shown in figure 2(*a*), the spatial flux in the overlap layer increases with Re and forms an outer peak given by the increasing energy injection due to the outer energy source.

3. Generalized Kolmogorov equation

The generalized Kolmogorov equation proposed by Hill (2002) is the balance equation for the second-order structure function, $\langle \delta u^2 \rangle$, where $\delta u^2 = \delta u_i \delta u_i$ and the fluctuating velocity increment is $\delta u_i = u_i(X_s + r_s/2) - u_i(X_s - r_s/2)$. According to its definition, $\langle \delta u^2 \rangle(r_i, X_i)$ depends both on the separation vector defined as $r_i = x_i' - x_i$ and on the location specified by the midpoint $X_i = (x_i' + x_i)/2$. Hereafter, index repetition implies summation. The second-order structure function can be interpreted as the amount of energy of a given scale r_s at a certain position in the flow X_s, and for that reason, hereafter, we will refer to the concept of scale energy. Let us note that, although $\langle \delta u^2 \rangle$ has the dimensions of kinetic energy and it is strictly related to the energy spectrum, the second-order structure function is not an intensive quantity. However, it represents the natural tool for the multiscale analysis of turbulent flows that lack a classical spectral decomposition due to violation of spatial homogeneity. The second-order structure function is defined in a four-dimensional space (r_x, r_y, r_z, Y_c) allowing one to distinguish fluxes between different wall distances Y_c and fluxes between different wall-normal scales r_y. This distinction would be missed by using the balance equation for spectral energy. The generalized Kolmogorov equation derives directly from the Navier–Stokes equations. For the symmetries of channel flow and considering increments r_s only in the directions parallel to the walls, $r_y = 0$ (Marati *et al.* 2004), the equation reads

$$\frac{\partial \langle \delta u^2 \delta u_i \rangle}{\partial r_i} + 2\langle \delta u \delta v \rangle \left(\frac{\mathrm{d}U}{\mathrm{d}y} \right)^* + \frac{\partial \langle v^* \delta u^2 \rangle}{\partial Y_c} = -4\langle \epsilon^* \rangle + 2\nu \frac{\partial^2 \langle \delta u^2 \rangle}{\partial r_i \partial r_i} - \frac{2}{\rho} \frac{\partial \langle \delta p \delta v \rangle}{\partial Y_c} + \frac{\nu}{2} \frac{\partial^2 \langle \delta u^2 \rangle}{\partial {Y_c}^2}. \tag{3.1}$$

Here $U(y)$ is the mean velocity profile, $Y_c = X_2$ is the wall-normal coordinate of the midpoint, asterisk denotes the arithmetic average at the points $X_s \pm r_s/2$ and $\epsilon = \nu(\partial u_i/\partial x_j)(\partial u_i/\partial x_j)$ is the pseudo-dissipation. Equation (3.1) involves a four-dimensional vector field, $\boldsymbol{\Phi} = (\Phi_{r_x}, \Phi_{r_y}, \Phi_{r_z}, \Phi_c)$, and can be restated as

$$\boldsymbol{\nabla}_4 \cdot \boldsymbol{\Phi}(\boldsymbol{r}, Y_c) = \xi(\boldsymbol{r}, Y_c), \tag{3.2}$$

where $\boldsymbol{\nabla}_4$ is the four-dimensional gradient and $\xi = -2\langle \delta u \delta v \rangle (\mathrm{d}U/\mathrm{d}y)^* - 4\langle \epsilon^* \rangle$ is the scale-energy source/sink given by the balance between production and dissipation. This equation allows one to identify the two transport processes occurring simultaneously in wall flows: the scale-energy transfer in the three-dimensional space of scales, $\boldsymbol{\Phi}_r = (\Phi_{r_x}, \Phi_{r_y}, \Phi_{r_z}) = \langle \delta u^2 \delta \boldsymbol{u} \rangle - 2\nu \nabla_r \langle \delta u^2 \rangle$, and the spatial energy flux among different wall distances, $\Phi_c = \langle v^* \delta u^2 \rangle + 2\langle \delta p \delta v \rangle/\rho - (\nu/2)\partial \langle \delta u^2 \rangle / \partial Y_c$. In the inertial subrange of homogeneous isotropic turbulence, (3.2) reduces to

$$\boldsymbol{\nabla}_3 \cdot \boldsymbol{\Phi}_r(\boldsymbol{r}) = -4\langle \epsilon \rangle, \tag{3.3}$$

where the contributions due to production, viscosity and spatial inhomogeneity are either negligible or zero. In this case, energy transport occurs only in the

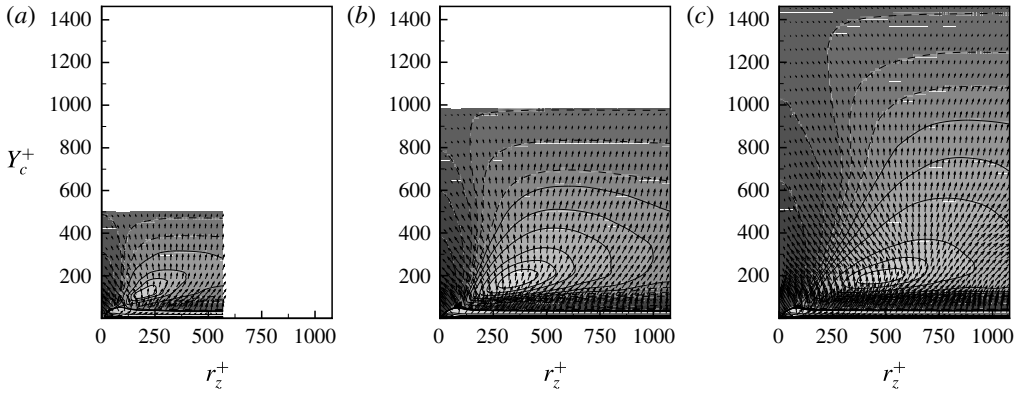

FIGURE 3. DNS of turbulent channel flows at (*a*) $Re_\tau = 550$, (*b*) $Re_\tau = 1000$ and (*c*) $Re_\tau = 1500$. Energy source, $\xi^+(r_x, r_z, Y_c)$, isolines; and field of fluxes, $(\Phi_{r_z}^+, \Phi_c^+)$, vectors in the $r_x = 0$ plane. Energy-source intensity increases from black to white. Solid lines denote positive values while dashed lines denote negative values.

space of scales, is radial and from large to small scales. The scale-energy source, $\xi_{hom} = \langle \delta u \delta f \rangle - 4\langle \epsilon \rangle$, where f is the external forcing, is a function only of the separation vector modulus $|\boldsymbol{r}|$ and it is always negative, $\xi_{hom} = g(|\boldsymbol{r}|) \leqslant 0$. In inhomogeneous flows, the turbulent production can locally exceed dissipation, leading to regions of scale-energy source in the augmented $(\boldsymbol{r}, Y_c)$ space where $\xi(\boldsymbol{r}, Y_c) > 0$. This is a distinguishing feature of actual inhomogeneous flows that has been shown in Cimarelli *et al.* (2013) to be responsible for a complex redistribution of scale energy where the controversial reverse energy cascade plays a central role. Hence, in what follows, the study of the Reynolds-number effects on the energetics of the flow will mainly focus on the behaviour of the source term ξ.

4. The structure of the source term

The topological structure of the source term obtained from the three DNS datasets shows that all the basic characteristics observed at the lowest Re_τ are also maintained at higher Reynolds numbers. By analysing the data in the reduced space (r_x, r_z, Y_c) for $r_y = 0$, the source ξ is found to reach its maximum at $r_x = 0$ in a range of small spanwise scales well within the buffer layer; see figure 3. This region of the reduced space is a singularity point for the fluxes. As more clearly seen in figure 4, the scale-energy flux vector field has its origin in this peak of scale-energy source, which can be considered as the engine of wall turbulence and will be hereafter called the driving scale range (DSR). The small-scale location of the scale-energy source actually violates the classical paradigm of homogeneous isotropic turbulence. In wall flows, the turbulent energy is generated amid the spectrum of turbulent fluctuations, not at the largest scales, and this fact leads to a complex redistribution of energy (Cimarelli *et al.* 2013), with strong consequences for turbulence modelling (Cimarelli & De Angelis 2012; Cimarelli & De Angelis 2014).

Another interesting feature emerging from the analysis of the Kolmogorov equation is the existence of a rescaled replica of the DSR, associated with a second peak in the scale-energy source, called hereafter outer driving scale range (ODSR). This outer peak of the scale-energy source has been observed in Cimarelli *et al.* (2013) and is present also at higher Reynolds numbers – see the isocontours of figure 3.

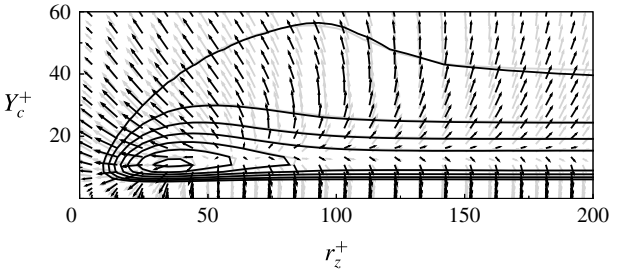

FIGURE 4. Scaling of the near-wall scale-energy source (ξ^+) and of the field of fluxes ($\Phi_{r_z}^+$, Φ_c^+) in the $r_x = 0$ plane. Grey isolines and vectors denote the $Re_\tau = 1000$ case while black ones denote the $Re_\tau = 1500$ case.

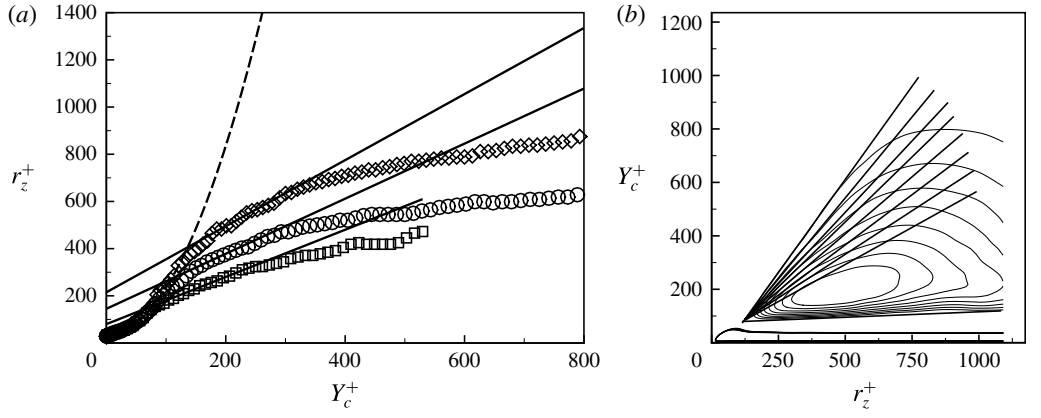

FIGURE 5. (*a*) Spanwise scale of maximum scale-energy source, $(\ell_z^{\xi_{max}})^+$, as a function of the wall distance. Diamonds denote the $Re_\tau = 1500$ case, circles the $Re_\tau = 1000$ case and squares the $Re_\tau = 550$ case. The dashed line denotes the quadratic increase near the wall, $(\ell_z^{\xi_{max}})^+ = 35 + 0.02Y_c^{+2}$, while the solid lines denote the linear increase in the overlap layer, $(\ell_z^{\xi_{max}})/h = 0.14 + (Y_c/h)$, $(\ell_z^{\xi_{max}})/h = 0.14 + 1.16(Y_c/h)$ and $(\ell_z^{\xi_{max}})/h = 0.14 + 1.4(Y_c/h)$, expressed in viscous units, i.e. $(\ell_z^{\xi_{max}})^+ = 80 + Y_c^+$, $(\ell_z^{\xi_{max}})^+ = 145 + 1.16Y_c^+$ and $(\ell_z^{\xi_{max}})^+ = 215 + 1.4Y_c^+$. (*b*) Energy source, ξ^+, isolines in the $r_x = 0$ plane for the $Re_\tau = 1500$ case. The straight lines are $r_z^+ = \gamma(\xi_0^+)\ (Y_c^+ - \tilde{Y}_c^+) + \tilde{r}_z^+$, where ξ_0^+ defines the iso-level of ξ, $\gamma(\xi_0^+) \in [0.04, 1.4]$, $\tilde{r}_z^+ = 120$ and $\tilde{Y}_c^+ = 80$.

4.1. *The driving scale range*

In agreement with the picture of a universal near-wall region, the geometrical properties of the DSR are unaffected by the Reynolds number; see figure 4. For the three cases considered, the source peak within the DSR is located at $(r_x^+, r_z^+, Y_c^+) = (0, 40, 12)$. This Reynolds-number invariance and the clear matching of scales and positions suggests a strong connection with the near-wall cycle. Note that, for a given wall distance, the source maximum ξ occurs at $r_x = 0$. Its location in the (r_z, Y_c) plane, reported in figure 5(*a*), defines the typical spanwise scale of the scale-energy source, $(\ell_z^{\xi_{max}})^+$. Near the wall, the spanwise location of the maximum increases quadratically with the wall distance, $(\ell_z^{\xi_{max}})^+ \approx 35 + 0.02Y_c^{+2}$, for all the Reynolds numbers considered. Clearly, within the DSR, for small distances from the

wall, $Y_c^+ < 30$, this trend results in an almost constant spanwise length scale: the typical spanwise scale of the most active structures of the wall is independent of the wall distance and Reynolds number. Although the topology of the DSR is basically *Re*-invariant, its intensity is not. The scale-energy source is found to increase slightly with Re_τ. In particular, we measure $\xi^+_{max} = 0.717$, 0.732 and 0.741 on moving from lower to higher Reynolds number. This trend is consistent with the commonly observed mixed inner/outer scalings of the near-wall quantities. In fact, it is thought that the outer dynamics actively modulates the near-wall turbulence by producing small-scale fluctuations increasing Reynolds number (Marusic *et al.* 2010*b*).

As shown by the vector field in figure 4, a direct consequence of the *Re* invariance of the topology of the scale-energy source term, ξ, is that also the scale-energy flux vector field, (Φ_{r_z}, Φ_c), remains identical for increasing Reynolds number, once rescaled in viscous units. In this scenario, the Reynolds-number effects should come only from the ODSR in the overlap region. Indeed, even if the observed second peak of scale-energy source ξ is very small compared to the one in the DSR, its relevance increases with *Re*, as will be discussed in the next sections.

4.2. *The outer driving scale range*

The ODSR belongs to the overlap layer and appears to be the result of a second outer turbulent production mechanism well separated from the near-wall dynamics. The ODSR is separated from the DSR by a scale-energy sink region. Interestingly, this separation is found to be more pronounced with increasing *Re*. The solid contour lines shown in figure 3 highlight that certain positive values for the source term ξ are shared by both the DSR and ODSR for $Re_\tau = 550$. On the contrary, for larger Reynolds numbers, the DSR and ODSR are more and more separated by negative values for the source term ξ, as shown by the number of dashed contour lines in between the inner and outer source shown in figure 3.

Although the peak intensity is smaller than the DSR one, the extent of the ODSR increases with *Re*, suggesting how this object can play an important role at large Reynolds numbers. In contrast with the DSR, where production is concentrated at small scales that are independent of Reynolds number, the ODSR involves larger scales and its extent in inner units increases with Re_τ. For the three Reynolds numbers considered, the peak of the ODSR occurs in a well-defined scale region expressed in outer units corresponding to $r_z/h \approx 0.34$. On the other hand, the physical location of the peak in the ODSR is $Y_c/h = (0.2; 0.18; 0.12)$ in outer units while $Y_c^+ = (112; 186; 192)$ in viscous units going from low to high Reynolds number. Contrary to the space of scales, r_z, which is found to be *Re*-invariant once expressed in outer units, the wall distances, Y_c, do not scale with *Re* in neither inner nor outer units. This behaviour is probably related to the fact that the overlap layer extends from a lower limit given in viscous units to an upper limit in outer units, e.g. for $100 < Y_c^+ < 0.2Re_\tau$, but the exact values are still a matter of scientific debate; see Marusic *et al.* (2010*b*) and references therein. These arguments suggest a mixed scaling with wall distance of the outer scale-energy source; see § 5 for a more detailed discussion. When considering the ODSR intensity, it is worth noting that the peak of scale-energy source in the ODSR remains essentially unaltered with Reynolds number once scaled in inner units and corresponds to $\xi^+ \approx 0.0095$.

The presence of the ODSR violates the equilibrium assumption of the overlap layer from which a local balance of production and dissipation is expected. Within the ODSR the energy injection is larger than the rate of dissipation, $\xi > 0$. As stated

by (3.2), this fact results in a positive divergence of the energy transfer, $\boldsymbol{\nabla}_4 \cdot \boldsymbol{\Phi} > 0$, which, under the assumption of a true equilibrium, is otherwise expected to be zero. This observation is consistent with the single-point energy excess already discussed in connection with figure 2 in § 2. Consequently, the overlap layer does not behave like a homogeneous shear flow traversed by a constant spatial flux of energy at both the single-point and two-point level. The ODSR continuously injects energy feeding the energy fluxes. As shown in figure 2, the spatial flux starts from the DSR in the buffer layer, it decreases by delivering energy in the sink layer wedged between the DSR and ODSR to increase again due to the energy injected by the ODSR leading to the second peak of the spatial flux. This second peak strongly depends on the Reynolds number, since the underlying physics of the ODSR belongs to the overlap layer whose extent, and, hence, its overall energy injection, increases with *Re*, as figure 3 clearly suggests.

In this context, the existence of a simple near-wall viscous scaling may be questioned by the fact that different turbulent engines with different characteristic scales are at work, thus leading to anomalous scaling. It is generally thought that the mixed inner/outer scaling is due to the fact that, with increasing Reynolds number, the large-scale structures of the overlap layer become more energetic and able to actively modulate the near-wall dynamics through production of near-wall fluctuations (Hutchins & Marusic 2007*b*; Mathis, Hutchins & Marusic 2009; Marusic, Mathis & Hutchins 2010*a*; Marusic *et al.* 2010*b*). Complementary to this picture, Jiménez (2012) describes this modulation as a local effect where small-scales structures equilibrate with their large-scale environment. From a point of view of scale-energy source and transfer, the mixed inner/outer scaling of the near-wall region could be interpreted as the result of a confinement of the scale-energy excess emerging from the near-wall region due to the presence of increasingly large production scales in the overlap layer. At given Reynolds number, the scale-energy flux originated in the DSR and directed towards the bulk of the flow encounters the additional energy source given by the ODSR. This additional energy source radiates scale energy and contributes to the overall energy flux. Below the ODSR the partial flux it generates is directed towards the wall, thereby opposing the flux produced in the DSR. The result is a net decrease in the flux towards the bulk. In fact, as stated by the turbulent kinetic energy and Kolmogorov equations (2.1) and (3.2), the source regions act to repulse the fluxes. Increasing the Reynolds number, the DSR remains fixed when scaled in inner units, while the effect of the ODSR increases. As shown in figure 3, the fluxes deviate to try to avoid the ODSR, which involves increasingly large scales with *Re*. Hence, the overall effect is a decrease with Reynolds number of the scale-energy flux from the near-wall region due to the presence of increasingly large production scales with *Re* in the ODSR. Accordingly, in the inset of figure 2(*a*) a decrease of the near-wall peak of the single-point spatial flux is observed at increasing *Re*. This decrease is compared with the ratio between the overall outer and inner energy sources in figure 6. By increasing the Reynolds number, the ratio Ξ_{out}/Ξ_{inn} increases and, as a consequence, the near-wall peak of the single-point spatial flux, ψ^+_{max}, significantly decreases. In conclusion, the scale-energy produced within the DSR increasingly feeds the turbulence in the near-wall region since the energy flux towards the channel centre is decreasing with *Re*. The resulting growth of the energy available near the wall is thus responsible for more intense fluctuations with *Re* leading to a mixed inner/outer scaling of near-wall quantities.

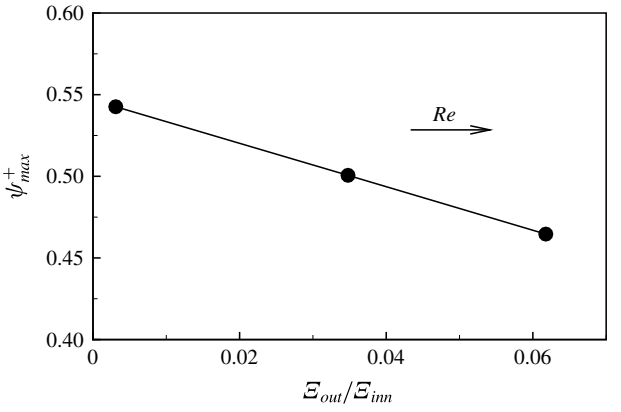

FIGURE 6. Behaviour of the near-wall peak of the single-point spatial flux, ψ^+_{max}, (2.1), as a function of the ratio Ξ_{out}/Ξ_{inn} for increasing Reynolds number.

5. Overlap layer scalings

Let us now investigate in more detail the peculiar features of the Kolmogorov equation within the overlap layer. The first point we address is the behaviour with wall distance of the spanwise scale of maximum scale-energy source for a given wall distance, $\ell_z^{\xi max}$. The present data show that, for the three Reynolds numbers considered, $\ell_z^{\xi max}$ increases almost linearly with Y_c; see figure 5(*a*). In particular, we observe $\ell_z^{\xi max}/h \sim 0.14 + Y_c/h$, $(\ell_z^{\xi max})/h \approx 0.14 + 1.16(Y_c/h)$ and $(\ell_z^{\xi max})/h \approx 0.14 + 1.4(Y_c/h)$ from low to high Reynolds numbers, respectively. This behaviour is similar to that reported in Saikrishnan *et al.* (2012) for the shear scale L_s, which is found to slightly increase its slope from $Re_\tau = 300$ up to $Re_\tau = 2000$, where it seems to asymptotically approach the dimensional prediction $L_s = ky$. In contrast to the slope, the intercept remains almost constant. This value of the intercept could be considered as the characteristic spanwise scale of the lower overlap layer. As shown by the isolines in figure 5(*b*) for $Re_\tau = 1500$, in the overlap layer the iso-levels of positive scale-energy source, $\xi > 0$, intercept spanwise scales that linearly increase with the distance from the wall. In particular, the iso-levels of ξ can be approximated by a sheaf of lines originating from a unique point at $\tilde{r}_z^+ = 120$ and $\tilde{Y}_c^+ = 80$ but with different slopes, i.e. $r_z^+ = \gamma(\xi_0^+)(Y_c^+ - \tilde{Y}_c^+) + \tilde{r}_z^+$, where ξ_0^+ defines the iso-level of ξ and $\gamma(\xi_0^+) \in [0.04; 1.4]$.

As already stated, the source maximum is found at $r_x = 0$ for all Y_c, while for $r_x > 0$ the source decreases; see figure 7(*a*). By tracking the spanwise scale of the maximum of ξ as a function of the streamwise scale, we find that these spanwise scales increase following a square-root law, $r_z^+ \sim \sqrt{r_x^+}$, independently of the Reynolds number. This behaviour is similar to that reported by del Alamo *et al.* (2004) for the spectral distribution of the Reynolds stresses and it finds a possible theoretical explanation in Moarref *et al.* (2013) in terms of geometrically self-similar resolvent modes. Since we observe that the spanwise scales involved in the scale-energy source increase linearly with wall distance, $r_z^+ \sim Y_c^+$, we argue that the streamwise scales should behave quadratically with wall distance, i.e. $r_x^+ \sim Y_c^{+2}$. Hence, we expect the scale-space behaviour of the scale-energy source of the ODSR in the overlap layer to be approximately self-similar if plotted as a function of r_x^+/Y_c^{+2} and r_z^+/Y_c^+. As shown in figure 7(*b*) this rescaling of ξ allows a unique comprehensive view of the

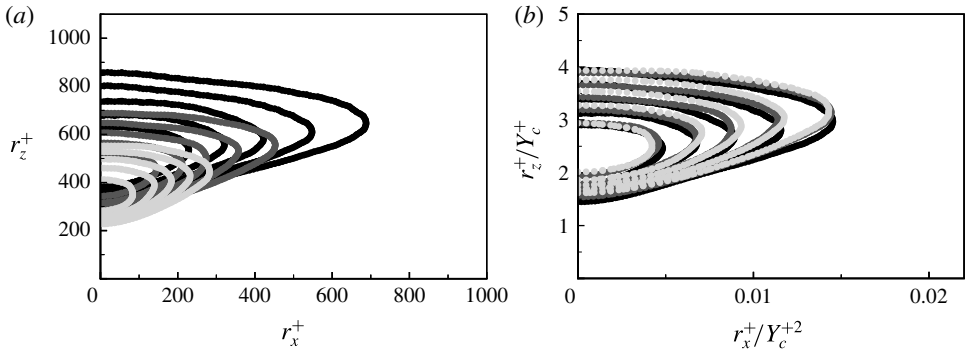

FIGURE 7. Scale-energy source isolines for three distances from the wall within the overlap layer for $Re_\tau = 1500$ ($Y_c^+ = 140$, light grey; $Y_c^+ = 180$, dark grey; and $Y_c^+ = 220$, black). (*a*) In inner units, the dimensions of the source region increase with the distance from the wall. (*b*) Spanwise and streamwise scales are normalized with the wall-normal distance and its square, respectively. Apparently, the isolines of the scale-energy source at different wall-normal distances tend to collapse one on top of the other.

outer scale-energy source where the Y_c dependence is dropped. The data we have available at other Reynolds numbers (not shown) suggest that this behaviour is Re_τ independent. The comparison with figure 7(*a*) highlights that this single picture of the overall behaviour of the outer scale-energy source would be missed when using viscous units. It is worth mentioning that the observed scale-space distribution of the outer scale-energy source, $r_z^+ \sim Y_c^+$ and $r_x^+ \sim Y_c^{+2}$, is consistent with the energy distribution found in Moarref *et al.* (2013), which, although different from the original scaling proposed by Townsend (1976), is explained by the conjecture of an overlap layer populated by self-similar structures attached to the wall (see e.g. del Alamo *et al.* 2006).

We address now the possibility to scale also the intensity of the outer scale-energy source, $\xi = -2\langle \delta u \delta v \rangle (\mathrm{d}U/\mathrm{d}y)^* - 4\langle \epsilon^* \rangle$. The rate of viscous dissipation is constant in the space of scales and can be easily modelled by means of the equilibrium hypothesis, $\langle \epsilon \rangle \sim u_\tau^3/\kappa y$. On the contrary, the scale-dependent behaviour of the production intensity is not trivial and needs a detailed analysis. Two distinct regimes are expected whose transition should be controlled by the shear scale ℓ_S (Jacob *et al.* 2008). For scales larger than ℓ_S, the prevailing mechanism that determines the scaling law is production. For scales smaller than ℓ_S, the energy cascade prevails and an isotropy-recovering behaviour is expected to occur. This range should be characterized by a power law with universal exponents based on the dimensional predictions proposed by Lumley (1965). As shown in figure 8(*a*) for $Re_\tau = 1500$ (the same behaviour is observed also for the lower Reynolds numbers considered), the scale-energy production follows the classical Lumley's prediction for the mixed structure function (Lumley 1965; Jacob *et al.* 2008), here extended to scale-energy production by taking into account the mean shear, $\mathrm{d}U/\mathrm{d}y$,

$$-2\langle \delta u \delta v \rangle \frac{\mathrm{d}U}{\mathrm{d}y} = \frac{\beta u_\tau^3 (r/y)^{4/3}}{\kappa y} \quad \text{for } r < \kappa y, \tag{5.1}$$

where κ is the von Kármán constant; see circles in figure 8(*a*). Production follows this power law for scales smaller than the shear scale ℓ_S as shown by the thick dash-dotted line in figure 8(*a*). The shear scale defined as $\ell_S = \sqrt{\epsilon/S^3}$, where $S = \mathrm{d}U/\mathrm{d}y$,

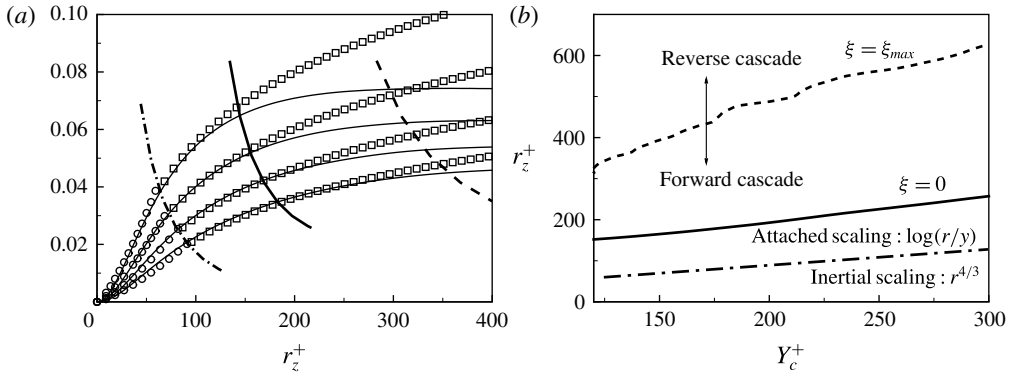

FIGURE 8. (*a*) Scaling of production, $-2\langle\delta u\delta v\rangle(\mathrm{d}U/\mathrm{d}y)$, for $r_x = 0$ and $Re_\tau = 1500$. From top to bottom the four solid lines provide the production at $Y_c^+ = 130$, 160, 190 and 230, respectively. Squares denote the logarithmic behaviour described by (5.2) and circles denote the inertial behaviour, (5.1). The three thick lines show the characteristic scales reported in panel (*b*). (*b*) The Y_c behaviour of the scale of maximum scale-energy source, $(\ell_z^{\xi_{max}})^+ \approx 215 + 1.4Y_c^+$ (dashed line), and of the zero scale-energy source, $(\ell_z^{\xi_{zero}})^+ \approx 80 + 0.65Y_c^+$ (solid line). The shear scale, $\ell_S^+ = \kappa Y_c^+$ (dash-dotted line), represents the cross-over between logarithmic and power-law scaling of production.

is computed here by using the overlap layer estimate, $\ell_S = \kappa Y_c$. Hence, the power law (5.1) is valid for scales smaller than the distance from the wall, the so-called detached scales. At scales larger than ℓ_S (attached scales), we find that the production in the overlap layer is well described by a logarithmic law,

$$-2\langle\delta u\delta v\rangle\frac{\mathrm{d}U}{\mathrm{d}y} = \frac{u_\tau^3(C + D\log(r/y))}{\kappa y} \quad \text{for } \kappa y < r < \ell_z^{\xi_{zero}}; \tag{5.2}$$

see squares in figure 8(*a*). This law is closely related to the (k^{-1}) law for the energy spectrum derived by Perry, Hanbest & Chong (1986); see also Nikora (1999). As shown in Davidson, Nickels & Krogstad (2006), the real-space analogue of the (k^{-1}) law is a logarithmic law for the streamwise second-order structure functions. Equation (5.2) represents an extension of this law to the mixed structure functions, $\langle\delta u\delta v\rangle$, which takes into account also the mean shear, $\mathrm{d}U/\mathrm{d}y$. Scaling (5.2) remains valid up to $r_z = \ell_z^{\xi_{zero}}$ where $\ell_z^{\xi_{zero}}$ is defined as the scale where the source term becomes zero, $\xi = 0$. For scales smaller than $\ell_z^{\xi_{zero}}$ the source term is actually a sink for the scale-energy fluxes, $\xi < 0$, while for larger scales it is a source, $\xi > 0$.

According to (3.2) and as shown by the vector field in figure 3, scales smaller than $\ell_z^{\xi_{zero}}$ are characterized by a negative divergence of the fluxes since $\xi < 0$ and, thus, by a forward cascade. As a consequence, the logarithmic behaviour (5.2) is associated with turbulent scales involved in a forward cascade process. Since, as anticipated, these scales are larger than $\ell_S = \kappa Y_c$, they are influenced by the presence of the walls. On the other hand, the power-law scaling characterizes scales smaller than $\ell_S = \kappa Y_c$. Hence, the influence of the wall should be somehow negligible and, consequently, the forward cascade should resemble the classical one proposed by Kolmogorov since an isotropic recovery should start to take place (see Casciola *et al.* 2005). It could be worth stressing that the shear scale, often identified with the distance from the wall, has long been addressed to explain the momentum and energy transfer between different scales of motion, starting from the pioneering work of Townsend (1976)

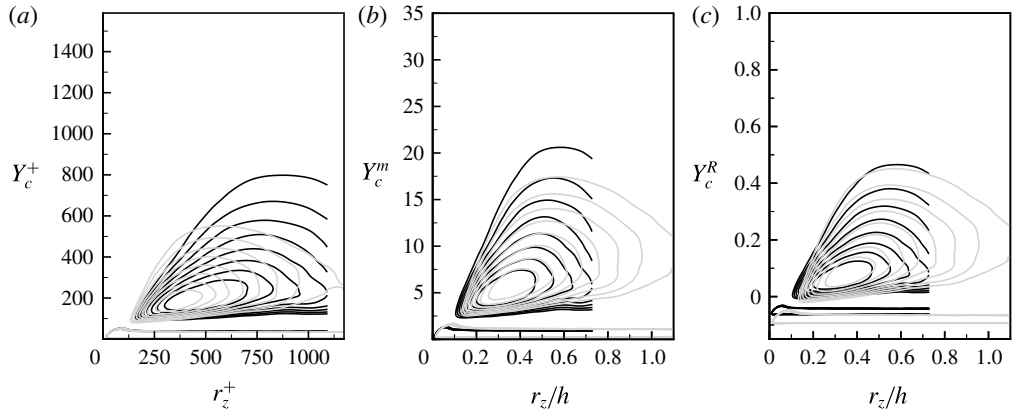

FIGURE 9. Energy source, ξ^+, isolines in the $r_x = 0$ plane for $Re_\tau = 1000$ (grey) and $Re_\tau = 1500$ (black): ξ^+ is shown as a function of (*a*) viscous quantity, (r_z^+, Y_c^+), (*b*) mixed quantity, $(r_z/h, Y_c^m)$, and (*c*) rescaled quantity, $(r_z/h, Y_c^R)$.

to more recent contributions (see e.g. Nikora 1999; Lozano-Duran & Jiménez 2014). As shown in figure 8(*b*), both ℓ_S and $\ell_z^{\xi_{zero}}$ linearly increase with the wall distance, denoting again statistical features attached to the wall. Since the slope of $\ell_z^{\xi_{zero}}$ is larger than that of the shear scale, ℓ_S, we can expect that the range of scales where the logarithmic scaling holds should expand significantly with Reynolds number, increasing the importance of the scaling for the prediction of production.

Figure 5 suggests a possible approximation for the source term for scales larger than $\ell_z^{\xi_{zero}}$. By assuming that the production term for scales close to $\ell_z^{\xi_{max}}$ roughly behaves linearly with r_z, see figure 8, we can model the source term as $\xi^+ \approx A(Y_c^+) r_z^+ + B(Y_c^+)$ since dissipation is a scale-independent process. In addition, we have also found in § 4.2 that the iso-levels of $\xi > 0$ form a sheaf of lines described by the equation $r_z^+ = \gamma(\xi_0^+)(Y_c^+ - \tilde{Y}_c^+) + \tilde{r}_z^+$, where ξ_0^+ defines the iso-level of ξ we are considering (see figure 5). By combining these two pieces of information, the slope γ is given by $\gamma(\xi_0^+) \approx G\xi_0^+ + H$, implying that the source term can be approximated as $\xi^+ \approx (r_z^+ - \tilde{r}_z^+)/G(Y_c^+ - \tilde{Y}_c^+) - H/G$. From our data we find $G = 103.9$ and $H = 0.58$.

Summarizing, we have shown that for a fixed Reynolds number the complex multidimensional features of the ODSR can be described in a simple way by using the self-similarity of the streamwise and spanwise scales shown in figure 7 and the scaling of the production intensity shown in figure 8. Despite the limited range of Reynolds numbers we have available, let us address now how this picture changes for different Reynolds numbers. As already shown in § 4.2, the intensity of the outer scale-energy source scaled in viscous units and its scale-space location scaled in outer units remain constant for the present Reynolds numbers. Hence, the effect of Reynolds number mainly reduces to an expansion/shrinking of the wall-normal distances. A sufficiently general procedure could be to consider a mixed scaling of the wall-normal distance in the form $Y_c^m = (Y_c/h)^\alpha (Y_c^+)^\beta$. Alternatively one could use outer units shifting the origin according to the expression $Y_c^R = (Y_c/h) - \eta^+/Re_\tau$, where η^+ is a free parameter. By considering $\alpha = \beta = 1/2$ in the first case and $\eta^+ = 100$ in the second one, the resulting scaling of the outer scale-energy source is shown in figure 9. Although not conclusive, given the small range of Reynolds numbers investigated, this result seems to be consistent with the possibility of a universal rescaling of the outer scale-energy source (ODSR).

6. Concluding remarks

By means of the description of turbulence given by the generalized Kolmogorov equation, we study the scale-energy transfer and production mechanisms of turbulent wall flows at different Reynolds numbers. Two driving mechanisms in terms of scale-energy source are identified for the fluxes. The first, stronger one, the driving scale range (DSR), belongs to the near-wall cycle. As expected, its inner-scaled topology remains unaltered with Reynolds number while its intensity is found to slightly increase with Re (near-wall modulation). The second outer scale-energy source, the outer driving scale range (ODSR), takes place further away from the wall in the overlap layer and is separated from the DSR by a distinct scale-energy sink layer, suggesting a possible independence of the production mechanisms of the ODSR from the near-wall region, which might be interpreted as an autonomous outer cycle. Although its intensity is small compared to the DSR, the outer region of scale-energy source expands with Reynolds number while its peak intensity remains almost constant. These observations suggest the importance of the ODSR for large-Reynolds-number wall turbulence.

Further analysis of the ODSR demonstrates that the Re dependence of the outer scale-energy source can be dropped by scaling in outer units the space of scales and in mixed units the wall distance, at least for the range of Reynolds numbers analysed here. Furthermore, we found that the spanwise scales involved in the scale-energy source linearly increase with the distance from the wall. On the other hand, the streamwise scales are connected to these spanwise scales of scale-energy source through a square-root law and, hence, quadratically increase with wall distance. These observations allow us to scale the outer scale-energy source, highlighting its self-similarities for different wall distances and Reynolds numbers. While considering the intensity of the outer scale-energy source, we found that the space of scales within the overlap layer can be divided into two distinct ranges. For scales larger than the shear scale, ℓ_s, but smaller than the cross-over scale of zero scale-energy source, $\ell_z^{\xi_{zero}}$, the outer scale-energy source follows a logarithmic law, $\xi = u_\tau^3(C + D\log(r/y) - 1)/\kappa y$. This behaviour is theoretically consistent with the presence of a k^{-1} law for the energy co-spectrum. For scales smaller than the shear scale, the outer scale-energy source follows a power law whose exponent equals Lumley's dimensional prediction, $\xi = u_\tau^3(\beta(r/y)^{4/3} - 1)/\kappa y$. These scales are involved in a direct cascade whose features should resemble the classical one since they are detached from the wall and, hence, an isotropic recovery is expected to take place. Interestingly, both $\ell_z^{\xi_{zero}}$ and ℓ_s increase linearly with wall distance. The different increase with wall distance of these two scales highlights the possible extension of the range of scales of validity of the logarithmic law for the prediction of outer scale-energy source at large Reynolds numbers. Overall, these observations suggest a strong connection of the observed outer scale-energy source with the presence of an outer turbulence production cycle whose statistical features agree with the hypothesis of an overlap layer dominated by self-similar structures attached to the wall.

The topology of the energy transfer is also studied. The paths of energy resemble the one reported in Cimarelli *et al.* (2013) for a lower-Reynolds-number case. Only one singularity point related to the DSR exists from which the fluxes depart also for larger Reynolds number. According to our observations we may expect a high-Reynolds-number state of wall turbulence where only one origin for the fluxes exists and corresponds to the DSR at the small scales of the near-wall region, since the intensity of the ODSR should be substantially Re independent. In this scenario, the Reynolds-number effects on the energy transfer should come only

from the expansion of the ODSR in both scale and physical space with Re. For increasing Reynolds numbers, the turbulent energy emerging from the DSR near the wall experiences an expanding outer scale-energy source in the overlap layer, which acts to repulse the fluxes as stated by (3.2). Hence, the fluxes try to avoid the increasingly large production scales of the ODSR and remain partially confined to the wall region, increasing the overall amount of energy locally available near the wall. Accordingly, we observe a decrease of the spatial flux from the buffer to the overlap layer at increasing Reynolds numbers. Hence we may conjecture that the near-wall modulation is a result of a confinement of the near-wall source due to the presence of increasingly large production scales in the overlap layer.

Acknowledgements

We acknowledge PRACE for awarding us via the REFIT project access to resource Jugene at the Jülich Supercomputing Centre in Germany. Computational resources at PDC were made available by SNIC. G.B. acknowledges financial support by the Swedish Research Council (grant number 621-2013-5784).

REFERENCES

DEL ALAMO, J. C., JIMÉNEZ, J., ZANDONADE, P. & MOSER, R. D. 2004 Scaling of the energy spectra of turbulent channels. *J. Fluid Mech.* **500**, 135–144.

DEL ALAMO, J. C., JIMÉNEZ, J., ZANDONADE, P. & MOSER, R. D. 2006 Self-similar vortex clusters in the turbulent logarithmic region. *J. Fluid Mech.* **561**, 329–358.

CASCIOLA, C. M., GUALTIERI, P., JACOB, B. & PIVA, R. 2005 Scaling properties in the production range of shear dominated flows. *Phys. Rev. Lett.* **95**, 024503.

CHEVALIER, M., SCHLATTER, P., LUNDBLADH, A. & HENNINGSON, D. S. (2007) SIMSON – a pseudo-spectral solver for incompressible boundary layer flows. *Tech. Rep.* TRITA-MEK 2007:07. KTH Mechanics, Stockholm, Sweden.

CIMARELLI, A. & DE ANGELIS, E. 2011 Analysis of the Kolmogorov equation for filtered wall-turbulent flows. *J. Fluid Mech.* **676**, 376–395.

CIMARELLI, A. & DE ANGELIS, E. 2012 Anisotropic dynamics and sub-grid energy transfer in wall-turbulence. *Phys. Fluids* **24** (1), 015102.

CIMARELLI, A. & DE ANGELIS, E. 2014 The physics of energy transfer toward improved subgrid-scale models. *Phys. Fluids* **26**, 055103.

CIMARELLI, A., DE ANGELIS, E. & CASCIOLA, C. M. 2013 Paths of energy in turbulent channel flows. *J. Fluid Mech.* **715**, 436–451.

DAVIDSON, P. A., NICKELS, T. B. & KROGSTAD, P. A. 2006 The logarithmic structure function law in wall-layer turbulence. *J. Fluid Mech.* **550**, 51–60.

DEGRAAFF, D. B. & EATON, J. K. 2000 Reynolds-number scaling of the flat-plate turbulent boundary layer. *J. Fluid Mech.* **422**, 319–346.

FLORES, O. & JIMÉNEZ, J. 2006 Effect of wall-boundary disturbances on turbulent channel flows. *J. Fluid Mech.* **566**, 357–376.

HAMILTON, J. M., KIM, J. & WALEFFE, F. 1995 Regeneration mechanisms of near-wall turbulence structures. *J. Fluid Mech.* **287**, 317–348.

HILL, R. J. 2002 Exact second-order structure–function relationship. *J. Fluid Mech.* **468**, 317–326.

HUTCHINS, N. & MARUSIC, I. 2007*a* Evidence of very long meandering streamwise structures in the logarithmic region of turbulent boundary layers. *J. Fluid Mech.* **579**, 1–28.

HUTCHINS, N. & MARUSIC, I. 2007*b* Large-scale influences in near-wall turbulence. *Phil. Trans. R. Soc. Lond.* A **365**, 647–664.

HWANG, Y. & COSSU, C. 2010 Self-sustained process at large scales in turbulent channel flow. *Phys. Rev. Lett.* **105**, 044505.

JACOB, B., CASCIOLA, C. M., TALAMELLI, A. & ALFREDSSON, H. P. 2008 Scaling of mixed structure functions in turbulent boundary layers. *Phys. Fluids* **20**, 045101.

JEONG, J., HUSSAIN, F., SCHOPPA, W. & KIM, J. 1997 Coherent structures near the wall in a turbulent channel flow. *J. Fluid Mech.* **332**, 185–214.

JIMÉNEZ, J. 2012 Cascades in wall-bounded turbulence. *Annu. Rev. Fluid Mech.* **44**, 27–45.

JIMÉNEZ, J. & HOYAS, S. 2008 Turbulent fluctuations above the buffer layer of wall-bounded flows. *J. Fluid Mech.* **611**, 215–236.

JIMÉNEZ, J. & PINELLI, A. 1999 The autonomous cycle of near-wall turbulence. *J. Fluid Mech.* **389**, 335–359.

KIM, H. T., KLINE, S. J. & REYNOLDS, W. C. 1971 The production of turbulence near a smooth wall in a turbulent boundary layer. *J. Fluid Mech.* **50**, 133–160.

LENAERS, P., LI, Q., BRETHOUWER, G., SCHLATTER, P. & ÖRLÜ, R. 2012 Rare backflow and extreme wall-normal velocity fluctuations in near-wall turbulence. *Phys. Fluids* **24**, 035110.

LOZANO-DURAN, A. & JIMÉNEZ, J. 2014 Time-resolved evolution of coherent structures in turbulent channels: characterization of eddies and cascades. *J. Fluid Mech.* **759**, 432–471.

LUMLEY, J. L. 1965 Interpretation of time spectra measured in high-intensity shear flows. *Phys. Fluids* **8**, 1056–1062.

MARATI, N., CASCIOLA, C. M. & PIVA, R. 2004 Energy cascade and spatial fluxes in wall turbulence. *J. Fluid Mech.* **521**, 191–215.

MARUSIC, I., MATHIS, R. & HUTCHINS, N. 2010*a* Predictive model for wall-bounded turbulent flow. *Science* **329**, 193–196.

MARUSIC, I., MCKEON, B. J., MONKEWITZ, P. A., NAGIB, H. M., SMITS, A. J. & SREENIVASAN, K. R. 2010*b* Wall-bounded turbulent flows at high Reynolds numbers: recent advances and key issues. *Phys. Fluids* **22**, 065103.

MATHIS, R., HUTCHINS, N. & MARUSIC, I. 2009 Large-scale amplitude modulation of the small-scale structures of turbulent boundary layers. *J. Fluid Mech.* **628**, 311–337.

MIZUNO, Y. & JIMÉNEZ, J. 2013 Wall turbulence without walls. *J. Fluid Mech.* **723**, 429–455.

MOARREF, R., SHARMA, A. S., TROPP, J. A. & MCKEON, B. J. 2013 Model-based scaling of the streamwise energy density in high-Reynolds-number turbulent channels. *J. Fluid Mech.* **734**, 275–316.

MONTY, J. P., STEWART, J. A., WILLIAMS, R. C. & CHONG, M. S. 2007 Large-scale features of turbulent pipe and channel flows. *J. Fluid Mech.* **589**, 147–156.

NAGIB, H. M. & CHAUHAN, K. A. 2008 Variations of von Karman coefficient in canonical flows. *Phys. Fluids* **20**, 101518.

NIKORA, V. 1999 Origin of the '−1' spectral law in wall-bounded turbulence. *Phys. Rev. Lett.* **83**, 734–736.

PERRY, A. E., HANBEST, S. M. & CHONG, M. S. 1986 A theoretical and experimental study of wall turbulence. *J. Fluid Mech.* **165**, 163–199.

PIOMELLI, U. & BALARAS, E. 2002 Wall-layer models for large-eddy simulations. *Annu. Rev. Fluid Mech.* **34**, 349–374.

ROBINSON, S. K. 1991 Coherent motions in the turbulent boundary layer. *Annu. Rev. Fluid Mech.* **23**, 601–639.

SAIKRISHNAN, N., DE ANGELIS, E., LONGMIRE, E. K., MARUSIC, I., CASCIOLA, C. M. & PIVA, R. 2012 Reynolds number effects on scale energy balance in wall turbulence. *Phys. Fluids* **24**, 015101.

SCHOPPA, W. & HUSSAIN, F. 2002 Coherent structure generation in near-wall turbulence. *J. Fluid Mech.* **453**, 57–108.

SMITH, C. R. & METZLER, S. P. 1983 The characteristics of low speed streaks in the near wall region of a turbulent boundary layer. *J. Fluid Mech.* **129**, 27–54.

SMITS, A. J., MCKEON, B. J. & MARUSIC, I. 2011 High-Reynolds number wall turbulence. *Annu. Rev. Fluid Mech.* **43**, 353–375.

TOWNSEND, A. A. 1976 *The Structure of Turbulent Shear Flow*. Cambridge University Press.